Towards encapsulation of nanoparticles in chabazite through interzeolite transformation

Rasmussen, Kristoffer Hauberg; Mielby, Jerrik Jørgen; Kegnæs, Søren

Published in:
ChemCatChem

Link to article, DOI:
10.1002/cctc.201800914

Publication date:
2018

Document Version
Peer reviewed version

Heterogeneous & Homogeneous & Bio- & Nano-
CHEMCATCHEM
CATALYSIS

Accepted Article

Title: Towards encapsulation of nanoparticles in chabazite through interzeolite transformation

Authors: Kristoffer Hauberg Rasmussen, Jerrik Mielby, and Soeren Kegnaes

To be cited as: *ChemCatChem* 10.1002/cctc.201800914

Link to VoR: http://dx.doi.org/10.1002/cctc.201800914

A Journal of
ChemPubSoc Europe

WILEY-VCH

www.chemcatchem.org

10.1002/cctc.201800914

WILEY-VCH

FULL PAPER

Towards encapsulation of nanoparticles in chabazite through interzeolite transformation

Kristoffer Hauberg Rasmussen[a], Jerrik Mielby[a], and Søren Kegnæs*[a]

Abstract: Encapsulation of Pt nanoparticles (1-2 nm) in the small pore zeolite chabazite (CHA) was achieved by a seed- and structure-directing agent-free interzeolite transformation from zeolite Y (FAU). Prior to the transformation, the Pt nanoparticles were encapsulated in the commercially available large pore zeolite H-Y by simple incipient wetness impregnation. The H-Y was then converted into CHA in a solution of KOH under hydrothermal conditions at 95 °C. All catalysts were characterized by XRD, N_2-physisorption, H_2-chemisorption, TEM and XPS and their catalytic activity were tested in CO oxidation. Although the catalytic activity of the encapsulated Pt nanoparticles decreased over time, it still remained more active than a reference catalyst prepared by impregnation. The thermal stability of the catalysts was investigated after calcination at 400 °C for 18 hours. Compared to the other catalysts, the encapsulated Pt nanoparticles only resulted in a small decrease in catalytic activity.

Introduction

Zeolites are microporous ordered structures with high surface areas.[1] Zeolites are extensively used in catalysis where they are used as catalysts or as a support material for metal ions or nanoparticles.[2,3] With more than 220[4] known framework structures combined with tunable chemical composition, zeolites provide a versatile support material for heterogeneous catalysts.[5] The use of zeolites as support for catalytically active metals offer several benefits. By encapsulating metal nanoparticles in the microporous cages and channels of the zeolite, it is possible to exploit the intrinsic shape selectivity of the framework.[6] Additionally, when confined in the microporous channels, the nanoparticles are more resistant towards sintering as well as being protected from larger poisonous species which can deactivate the catalyst.[7-10]

Recently, the small pore zeolite chabazite (CHA) has attracted attention due to the high thermal stability and resistance towards dealumination and migration.[11–13] Encapsulation of Pt in CHA has shown to be useful in exhaust gas purification[14] and selective in hydrogenation of ethylene compared to propylene[15].

[a] K. H. Rasmussen, Dr. J. Mielby, Prof. S. Kegnæs*
Department of Chemistry,
Technical University of Denmark
Kemitorvet 207, 2800 Kongens Lyngby, Denmark
E-mail: skk@kemi.dtu.dk

Supporting information for this article is given via a link at the end of the document.

CHA is typically synthesized with the aid of an organic structure directing agent (OSDA), such as *N,N,N*-Trimethyl-1-ammonium adamantine or benzyltrimethylammonium which are relatively costly.[13,15–20] CHA can also be obtained through interzeolite transformation. In particular, FAU has been used to obtain CHA, however, LEV and GIS have also shown to be successful starting zeolite. Low Si/Al ratio CHA can be obtained without the use of seed crystals and OSDA, however, these are necessary in order to obtain CHA crystals with higher Si/Al ratios.[21–30] It is proposed, that the structural similarities between the zeolites act as a driving force for the crystallization, thus shortening the crystallization time.[31,32]

Encapsulation of metal nanoparticles are often accomplished by post-synthetic modifications such as impregnation or ion-exchange[33], however, these are not efficient for CHA due to its small pores.[34,35] Metals can sometimes be incorporated in zeolites during the synthesis using strongly coordinating ligands that prevent precipitation and ensures interactions between the forming zeolite and the metal precursor.[6,15,36–40] The difficulty of introducing metal nanoparticles in small pore zeolites may be overcome by using a large pore zeolite as a starting material. By introducing metal nanoparticles into the parent large pore zeolite, and convert it into a more dense daughter zeolite with smaller pores could offer an alternative route for encapsulation of the metal in the small pore zeolite. This approach was recently demonstrated by Iglesia *et al*., who developed synthetic routes for metal encapsulation in a parent zeolite which then could be converted into a daughter zeolite (MFI and ANA) while retaining the encapsulation of the nanoparticles.[31,39] Expansion of the zeolite framework structures that can be accessed through this synthesis approach without the use of a structure directing agent or seed crystals still remains a challenge.[20,41–45]

Here, we report a simple procedure for introducing Pt nanoparticles in CHA zeolite through an interzeolite transformation from large pore FAU zeolite without the use of OSDAs or seed crystals. Our synthesis strategy exploit a commercially available zeolite Y which readily can be impregnated with a Pt precursor and easily transformed into CHA with partial retention of the encapsulated metal nanoparticles. A complete overview of the presented synthesis approaches are illustrated in Figure 1.

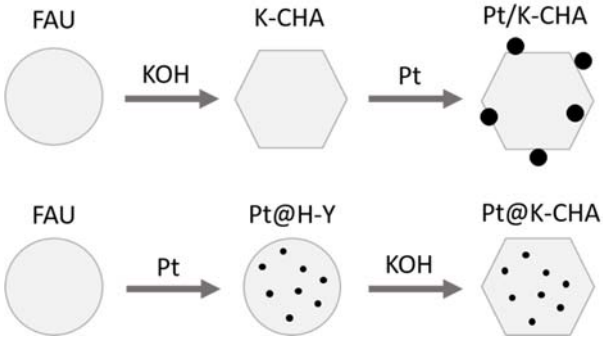

Figure 1. CHA zeolite (hexagon) produced in OSDA-free synthesis from FAU zeolite (circle). Pt was introduced by incipient wetness impregnation.

Results and Discussion

Characterization

Encapsulated Pt nanoparticles in H-Y zeolite (Pt@H-Y) was obtained by an incipient wetness impregnation of commercially available H-Y. Similar, as a reference, Pt nanoparticles on K-CHA (Pt/K-CHA) was obtained by an incipient wetness impregnation of synthesized K-CHA. Encapsulated Pt nanoparticles in K-CHA (Pt@K-CHA) was obtained from an interzeolite transformation of Pt@H-Y. X-ray powder diffraction patterns were obtained for the three materials which is shown in Figure 2. The diffraction patterns of the three materials (Figure 2 top) are consistent with a FAU structure for Pt@H-Y and a CHA structure for both Pt@K-CHA and Pt/K-CHA.[4,46–48] To evaluate the size of the Pt particles Figure 2 bottom shows a zoomed part of the diffraction pattern. From Figure 2 bottom, it is clear that only Pt/K-CHA shows peaks related to Pt. No peaks from Pt in the diffraction patterns for Pt@H-Y and Pt@K-CHA were observed. This indicates that the Pt particles in Pt@H-Y and Pt@K-CHA are relative small and that the Pt particles do not grow during the interzeolite transformation. The distinct diffraction peaks from Pt in the pattern for Pt/K-CHA clearly supports that the Pt particles obtained from the direct impregnation of K-CHA leads to larger particles compared to the other two materials. This suggest that the encapsulation of the Pt particles was not successful by the direct impregnation of the small pore CHA zeolite.

X-ray fluorescence (XRF) was used to determine the Si/Al ratio and the Al/K ratio in the materials. The results are shown in supporting information.

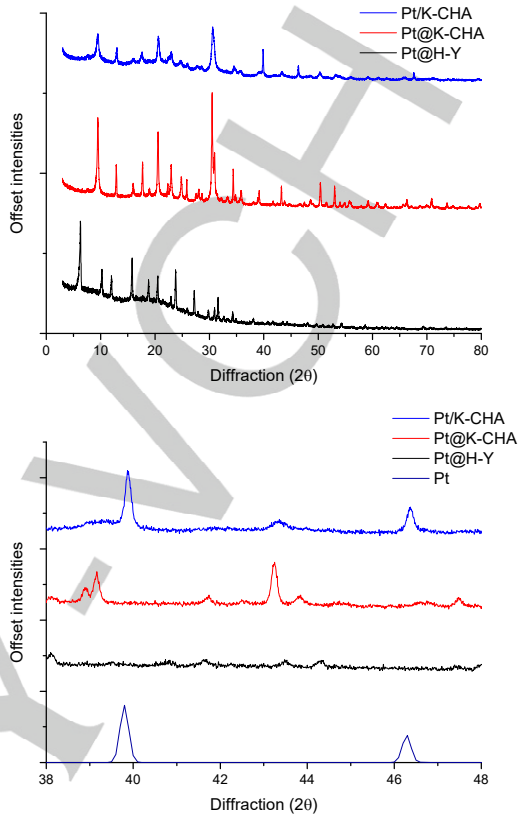

Figure 2. XRPD pattern for the synthesized materials (top) and a zoomed area of Pt@H-Y, Pt@K-CHA, and Pt/K-CHA with reference peaks from Pt[49] (bottom).

To determine the amount of platinum in Pt@H-Y, Pt@K-CHA, and Pt/K-CHA, ICP analysis was performed which showed a Pt wt% of 0.86, 0.65, and 0.95 respectively. Based on ICP, it is clear that a substantial amount of the Pt stays incorporated in the zeolite materials during interzeolite transformation from H-Y to K-CHA zeolite. However, part of the Pt is lost during the interzeolite transformation properly due to part of the zeolite materials being dissolved in the process. The wt% of Pt in the two materials (Pt@H-Y and Pt@K-CHA) should be more or less equal and directly comparable since the partial loss of SiO_2 in the zeolite transformation is compensated by the uptake of K^+ as extra framework cation.

The porosity of the obtained materials was measured by N_2 physisorption. Physisorption isotherms of Pt@H-Y, Pt@K-CHA and Pt/K-CHA can be seen in figure 3. The physisorption isotherm of Pt@H-Y indicates that the material is microporous due to the large uptake of N_2 at relative pressures below 0.02. As expected, the physisorption isotherms of Pt@K-CHA and Pt/K-CHA indicates a rather non-porous structure. This low porosity of K-CHA materials have been reported by several research groups.[50,51] Ridha *et al.*[50] proposed that the potassium ion

10.1002/cctc.201800914

restrict the accessibility of N_2 to the pores of chabazite. The accessibility of the K-CHA is dependent on the temperature and the type of gas.[50,51] Ridha *et al*. showed that the K-CHA was almost inaccessible to N_2 whereas CO_2 could access the channels in K-CHA. This was ascribed to a difference in the polarizability and quadrupole moment. Additionally, they showed that the pores were inaccessible for N_2 at 77 K but accessible at 273 K. [50] It is possible to restore the porosity of CHA (determined by N_2 physisorption) by ion-exchange to the H-form with NH_4NO_3 (see supporting information figure S2).

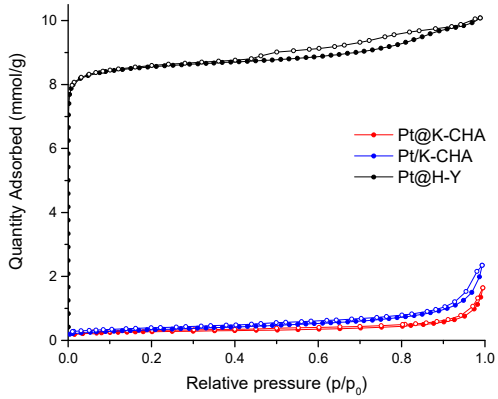

Figure 3. N_2 physisorption of Pt@H-Y, Pt@K-CHA, and Pt/K-CHA.

The stability of the zeolites with Pt (Pt@H-Y, Pt@K-CHA, and Pt/K-CHA) were tested by heating them in air at 400 °C for 18 h (400-Pt@H-Y, 400-Pt@K-CHA, and 400-Pt/K-CHA). The results from N_2 physisorption of all the samples including the Pt free zeolites are summarized in table 1. The results show that neither calcination at 400 °C nor introduction of Pt in the supports have a significant effect on surface area and porosity.

Table 1. Nitrogen physisorption data for the catalytic supports and the prepared samples. The data were obtained at 77 K.

Sample	V_{micro} (cm^3/g)[a]	V_{total} (cm^3/g)[b]	Surface area (m^2/g)[c]
H-Y	0.27	0.34	762
Pt@H-Y	0.27	0.34	765
K-CHA	0.003	0.03	25
Pt@K-CHA	0.003	0.03	22
Pt/K-CHA	0.001	0.04	27
400-Pt@H-Y	0.27	0.35	773
400-Pt@K-CHA	0.002	0.04	26
400-Pt/K-CHA	0.0002	0.04	24

[a] Calculated by t-plot method. [b] Calculated from a single point adsorption at 0.95 relative pressure. [c] Calculated by the BET method. The very low porosity of chabazite is due to K^+ blocking the channels[50].

To evaluate the effect of impregnation before or after interzeolite transformation, Pt@H-Y, Pt@K-CHA, and Pt/K-CHA were analyzed by transmission electron microscopy (TEM). Representative images from the TEM analysis of the three samples are presented in Figure 4. The image of Pt@H-Y (Figure 4A) clearly shows that the Pt nanoparticles are of uniform size and well distributed throughout the crystals. After interzeolite transformation, zeolite crystals with well distributed small Pt nanoparticles were also obtained for Pt@K-CHA (figure 4B). However, some crystals were the Pt nanoparticles have agglomerated were also observed (figure 4C). The inconsistent capture of the nanoparticles in the formed CHA zeolite framework is likely due to a too fast dissolution rate of the FAU parent zeolite compared to the recrystallization rate to the CHA daughter zeolite. We speculate that a better control on the dissolution/recrystallization rates could improve the particle dispersion.

The size of the Pt individual particles, however, seems to be retained in both the agglomerated and well distributed zeolite crystals. TEM analysis of the obtained materials show a variation of the metal loading among the different zeolite crystals. See supporting information for additional TEM images of Pt@H-Y and Pt@K-CHA. The variation in metal loading has previously been observed by Zečević *et al*.[52] for 1 wt% Pt in zeolite Y crystals. Zečević *et al*.[52] found that the metal loading may vary by a factor of up to 35 between the different zeolite Y crystals.

From the TEM image of Pt/K-CHA (figure 4D), it is clear that the particles are much larger and less distributed, which shows that the impregnation of the K-CHA is not a suitable way for encapsulation of Pt nanoparticles in the small pore CHA framework.

10.1002/cctc.201800914

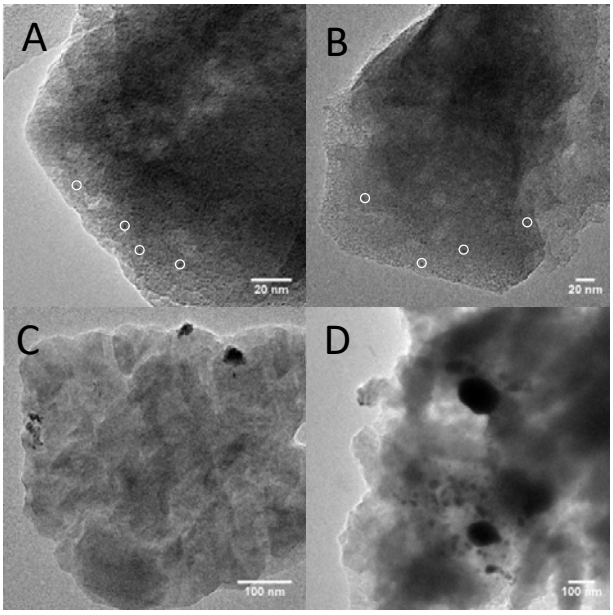

Figure 4. TEM images of Pt@H-Y (A), Pt@K-CHA (B + C), Pt/K-CHA (D).

The average size of the Pt nanoparticles was determined by H_2 pulse chemisorption. For Pt@H-Y, the average size of the Pt was found to be 1.0 nm, which is consistent with the TEM images of the materials. For Pt@K-CHA, based on TEM images, the Pt particles are approximately the same size as for Pt@H-Y. Unfortunately, this is difficult to verify by H_2 pulse chemisorption, (see supporting information). For Pt/K-CHA, the average particle size of Pt was 8.7 nm, which show the unsuccessful encapsulation of Pt in K-CHA results in much larger Pt particles Pt@H-CHA could be obtained by ion-exchange of Pt@K-CHA with NH_4NO_3, however, this result in Pt particles growth (see supporting information).

X-ray photoelectron spectroscopy was used to evaluate the encapsulation of Pt nanoparticles in the zeolite crystals (see figure 5). For Pt@H-Y, it is not possible to distinguish the Pt signal from the background-noise, thus, the Pt nanoparticles are in fact encapsulated in the H-Y crystal. The XPS spectrum for Pt@K-CHA and Pt/K-CHA both show the 4d peaks from Pt. This fits well with the TEM images of the materials, which show either large particles for Pt/K-CHA and some agglomeration for Pt@K-CHA which are likely on or close to the surface respectively.

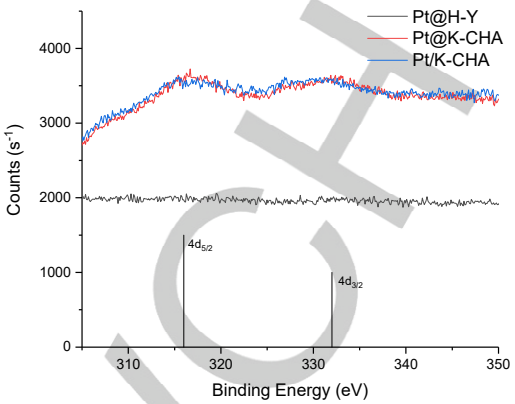

Figure 5. XPS of 4d orbitals of Pt@H-Y, Pt@K-CHA, and Pt/K-CHA. The approximate position of the 4d orbitals for Pt are shown as lines.

Catalytic tests

The catalytic activity of the synthesized materials were tested in CO oxidation. The CO oxidation as a function of temperature is shown in Figure 6. Figure 6 shows a slow increase in the conversion of CO to CO_2 until approximately 45 % conversion where the light of temperature is reached and from there the conversion increases rapidly to 99-100 %.

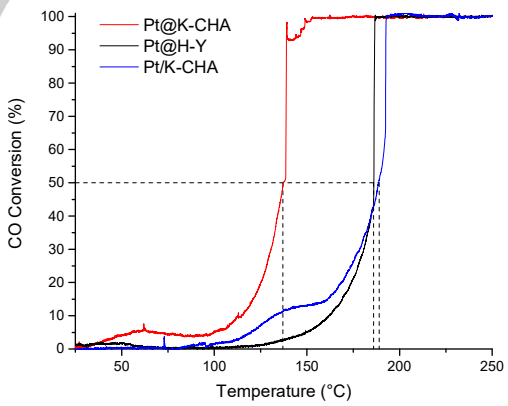

Figure 6. CO oxidation profile for Pt@H-Y, Pt@K-CHA, and Pt/K-CHA with dashed lines showing the 50 % conversion temperatures.

The 50 % conversion temperature for the different catalysts are listed in table 2. Additionally, the turn over frequency at 137 °C, which is the 50% conversion temperature of the most converting catalyst, Pt@K-CHA, is shown in table 2. The pure zeolite material,

H-Y(5.1) and K-CHA, as well as pure quartz did not show any catalytic activity in CO oxidation (see Supporting information), hence, the catalytic activity is due to the Pt metal. An additional reference material where Pt was introduced into K-CHA (IE-Pt/K-CHA) by ion-exchange showed a significantly lower catalytic activity compared to the other tested materials (see supporting information).

Table 2. Catalytic results for CO oxidation

Entry	Sample	50 % conv. (°C)[a]	wt% Pt[b]	TOF (CO/ $Pt_{surface}$ * min))[c]
1	Pt@H-Y	186	0.86	0.6
2	Pt@K-CHA	137	0.65	5.6[d]
3	Pt/K-CHA	188	0.95	7.2

[a] 50 mg catalyst [b] Measured by ICP-OES [c] Obtained at 50% conversion temperature for Pt@K-CHA (137 °C) with surface area of Pt from H_2-pulse [d] Size of Pt particles based on TEM analysis was estimated to be the same size as for Pt@H-Y, due to inaccessible measurement by H_2-pulse.

The catalytic results show that Pt@K-CHA is the most active catalyst in CO oxidation. Pt@K-CHA is a significantly better catalyst for doing the CO oxidation compared to the Pt/K-CHA, thus, indicating that the smaller metal nanoparticles encapsulated in CHA increase the activity of the material. The superior catalytic activity for Pt@K-CHA compared to Pt@H-Y (~50 °C difference) is likely due to a promotion effect of a potassium ion compared to a proton. This promotion effect of alkali metal ions in CO oxidation has previously been addressed by Visser et al.[53] who found that the catalytic activity of Pt in zeolite Y was higher for K^+ ions compared to protons as extra framework ions. The enhanced effect of the catalytic activity was ascribed to the basic properties of the K^+ ion compared to the H^+, resulting in higher electron density on the Pt particles and, thus, higher catalytic oxidation of CO.

Stability tests

The stability of the catalysts where tested by heating Pt@H-Y, Pt@K-CHA and Pt/K-CHA in air at 400 °C for 18 h. The catalysts were tested for CO oxidation directly after calcination since no significant effect of the reduction was observed for the catalytic results. Additionally, the materials stability were tested over several consecutive CO oxidation cycles (see supporting information for an example with 400-Pt@H-Y in the cycled experiment). The results from the tests are listed in Table 3.

Table 3. Catalytic results for CO oxidation in stability tests

Entry	Sample	50 % conv./ °C (1^{st})	50 % conv./ °C (4^{th})
1	Pt@H-Y	186	187
2	Pt@K-CHA	137	189
3	Pt/K-CHA	188	202
4	400-Pt@H-Y	191	187
5	400-Pt@K-CHA	140	178
6	400-Pt/K-CHA	202	203

For both the Pt@H-Y and 400-Pt@H-Y, the catalysts do not seem to lose activity over consecutive cycles for CO oxidation since both materials show similar catalytic activity. For Pt@K-CHA and Pt/K-CHA, both materials lose activity over the cycles. Pt@K-CHA drops in activity to a level comparable to Pt@H-Y but still outperforms Pt/K-CHA. For 400-Pt@K-CHA, the material is actually more active after four cycles compared to Pt@K-CHA. This could be explained by a redispersion of Pt during calcination at 400 °C, which was addressed by Moliner et al.[15] This is in contrast to Pt/K-CHA, which has a decreased activity already from the first cycle. From these experiments, it may seem that the particles located on the external surface do not redisperse under the thermal treatment.

Figure 7 shows TEM images of used Pt@H-Y and Pt@K-CHA after 4 cycles of CO oxidation. The TEM images look similar to the images before catalysis, with only a slight increase in the Pt particle size in Pt@H-Y. For Pt@K-CHA it is hard to determine if the particles have grown during analysis due to the agglomeration.

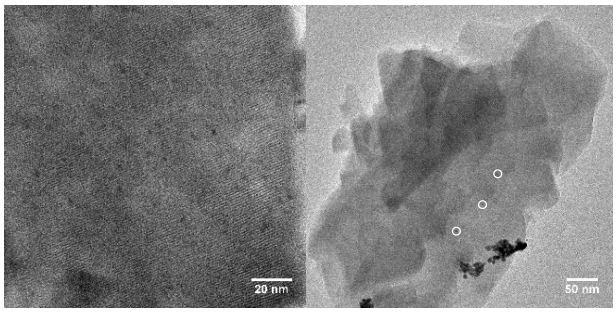

Figure 7. Used Pt@H-Y (left) and used Pt@K-CHA (right) after four consecutive CO oxidation cycles.

Conclusions

A new and easy method for obtaining small nanoparticles of Pt in CHA was developed. The synthesis approach utilize a commercially available zeolite Y as which can be interconverted to CHA without the use of an OSDA. Pt was introduced in the H-Y(5.1) which yielded small and well distributed NPs which then was converted to Pt encapsulated in CHA with partial retention of the particles size but with varying distribution of the nanoparticles. Pt@K-CHA obtained from the interzeolite transformation showed to be the most active of the synthesized materials in CO oxidation. This is likely due to a promotion effect from the potassium cation when comparing against Pt@H-Y. It is, however, still superior to Pt/K-CHA which was obtained from the direct impregnation of K-CHA.

Experimental Section

Characterization

X-ray powder diffraction patterns were recorded on a STOE STADI P in transmission mode using Cu –Kα_1 radiation from a curved germanium (111) monochromator and a 5° linear gas detector measuring in the 2θ interval 3-80° in steps of 0.01°. Nitrogen adsorption and desorption measurements were performed at liquid nitrogen temperature (77 K) on a Micromeritics ASAP 2020. The samples were degassed in vacuo at 200 °C prior to measurement. Total surface area was calculated according to the BET method. Micropore volumes was determined by the t-plot method. Transmission electron microscopy (TEM) was performed on FEI Tecnai T20 G2 microscope operating at 200 kV. The samples were dispersed directly on a holey carbon grid. Pulse chemisorption was performed on a AutoChem II 2920 with a TCD detector. The sample was dried under vacuum at 50 °C overnight prior to analysis. For analysis, the sample (typically 0.2-0.4 g) was heated in H_2 (2.5 % in Ar, 50 mL/min, AGA) to 120 °C for 30 min, then 220 °C for 30 min, and lastly 400 °C for 2 h with 10 °C/min ramping in between the plateaus. Chemically adsorbed H_2 was removed by heating at 400 °C in Ar (50 mL/min) for 90 min. The sample was cooled to ambient temperature and then heated to 45 °C for pulsing. The sample was subjected to pulses of H_2 (5 % in Ar, 0.5 mL) in an Ar flow (50 mL/min) every 3.5 min. Dispersion and size of the nanoparticles were calculated based on the stoichiometric 1:1 $H:M_{surface}$ of irreversible chemisorbed H_2.[54] ICP-OES was performed on an iCAP 7000 Plus Series from Thermo Scientific equipped with a Teledyne CETAC ASX-560 autosampler. The Pt containing zeolites (about 100 mg) were dissolved in *aqua regia* at 90 °C for 30 min. The samples were filtered and diluted to 250 mL in a volumetric flask. A calibration curve for Pt was obtained immediately prior to analysis. X-ray photoelectron spectroscopy (XPS) was performed on a ThermoFischer Scientific K-Alpha™ with a monochromated Al Kα X-ray source. The analysis was performed at pressures around $2 \cdot 10^{-7}$ mbar. The spectra were recorded with 0.1 eV steps and with a pass energy of 50 eV and a spot size of 400 µm. 50 scans were performed for elemental analysis. X-ray Fluorescence (XRF) was performed on a PANalytical Epsilon 3X. Glass discs was made using a Claisse LeNEO Fluxer. The glass discs consisted of around 250 mg sample, 10.5 g lithium metaborate/tetraborate and about 60 mg LiBr as non-wetting agent.

Materials and synthesis

All reagents were of reagent grade and used without further purifications: CBV400 (H-Y(5.1) (SiO_2/Al_2O_3), Zeolyst), KOH (90%, Sigma-Aldrich), $H_2PtCl_6 \cdot 6H_2O$ (37.5 % Pt, Sigma-Aldrich), $Pt(NH_3)_4(NO_3)_2$ (50 % Pt, Sigma-Aldrich), Quartz (Sigma-Aldrich). **Synthesis of K-CHA:** K-CHA was obtained by following a procedure reported by Bourgogne et al.[55] where water (7.93 mL) and a KOH solution (45%, 1.07 mL) were mixed with 1 g of zeolite in a high density polyethylene bottle (Frisenette). The mixture was shaken for 30 s before it was heated in an oven at 95 °C for 96 hours, filtered while hot and washed with water until neutral pH of washing-water. The solid was dried at 80 °C overnight. The successful formation of CHA from FAU is dependent on both the presence of K^+ and the Si/Al ratio.[24,30] **Pt@H-Y and Pt/K-CHA**: H-Y(5.1) and K-CHA were dried in vacuo overnight before incipient wetness impregnation. H-Y(5.1) was impregnated with an aqueous solution of H_2PtCl_6 corresponding to 90 % of the total volume determined by nitrogen physisorption. Due to a low pore volume of K-CHA obtained from N_2 physisorption, an appropriate amount of water for impregnation was approximated by adding water to dried K-CHA to a wetness degree similar for what was seen for H-Y(5.1). The concentration of H_2PtCl_6 was adjusted to give a 1 wt% Pt loading in both H-Y(5.1) and K-CHA. The impregnated zeolites were dried at 100 °C for 24 h hours before they were calcined at 350 °C for 2 hours with a 0.5 °C/min heating ramp. The calcined samples was reduced under pure H_2 at 600 °C for 3 hours with a 5 °C/min ramp. The samples were denoted Pt@H-Y and Pt/K-CHA respectively. **Pt@K-CHA**: Pt@K-CHA was obtained by following the same procedure as for K-CHA with the change of H-Y(5.1) to Pt@H-Y.

Catalytic test and stability

CO oxidation: CO oxidation was measured in a plug flow setup. 50 mg of fractionated catalyst (180-355 µm) was diluted with 100 mg of quartz (180-355 µm) and placed in a tubular quartz reactor (diameter 4 mm) fixed by two pieces of glass wool. A thermocouple was placed just after the catalytic

bed to measure and control the temperature of the catalyst. The activity was tested by flowing 1 % CO in 78.3 % N_2 and 20.7 % O_2 (AGA, 50 mL/min) controlled by a Brooks 4800 series mass flow controller and increasing the temperature of the catalyst bed to 250 °C by 2 °C min^{-1}. The concentration of CO and CO_2 was measured with a Rosemount BINOS 100 with a non-dispersive infrared detector for both gasses. The gas was preheated by passing through the heating block before it entered the tubular quartz reactor.

Stability of catalysts: To test the stability of the catalysts, Pt@H-Y, Pt@K-CHA, and Pt/K-CHA were calcined in a muffle oven at 400 °C for 18 h with a 1 h temperature ramp from ambient to 400 °C. The samples were denoted 400-Pt@H-Y, 400-Pt@K-CHA, and 400-Pt/K-CHA respectively. The catalyst stability was additionally tested by heating to 250 °C and then cooled to 50 °C four consecutive times with a heating and cooling ramping temperature of 2 °C min^{-1}.

Acknowledgements

The authors gratefully acknowledge the support of from Independent Research Fund Denmark (grant no. 6111-00237), Villum Fonden (grant no.13158) and from Haldor Topsøe A/S.

Conflict of interest

The authors declare no conflict of interest.

Keywords: Zeolites • Encapsulation • Platinum • Interzeolite transformation • Chabazite

[1] J. Čejka, S. Mintova, *Catal. Rev.* **2007**, *49*, 457–509.
[2] C. Martínez, A. Corma, *Coord. Chem. Rev.* **2011**, *255*, 1558–1580.
[3] A. Corma, *Chem. Rev.* **1995**, *95*, 559–614.
[4] International Zeolite Association Structure Commission, "Database of Zeolite Structures," can be found under http://www.iza-structure.org/databases/, **2017**.
[5] G. Ertl, H. Knözinger, F. Schüth, J. Weitkamp, Eds. , *Handbook of Heterogeneous Catalysis. 2nd Edition (Second, Completely Revised and Enlarged)*, Wiley-VCH, Weinheim, **2008**.
[6] A. B. Laursen, K. T. Højholt, L. F. Lundegaard, S. B. Simonsen, S. Helveg, F. Schüth, M. Paul, J.-D. Grunwaldt, S. Kegnaes, C. H. Christensen, et al., *Angew. Chemie* **2010**, *122*, 3582–3585.
[7] B.-Z. Zhan, E. Iglesia, *Angew. Chemie Int. Ed.* **2007**, *46*, 3697–3700.
[8] J. Mielby, J. O. Abildstrøm, F. Wang, T. Kasama, C. Weidenthaler, S. Kegnaes, *Angew. Chemie Int. Ed.* **2014**, *53*, 12513–12516.
[9] K. T. Højholt, A. B. Laursen, S. Kegnæs, C. H. Christensen, *Top. Catal.* **2011**, *54*, 1026–1033.
[10] F. Goodarzi, L. Kang, F. R. Wang, F. Joensen, S. Kegnæs, J. Mielby, *ChemCatChem* **2018**, *10*, DOI 10.1002/cctc.201701946.
[11] P. G. Blakeman, E. M. Burkholder, H.-Y. Chen, J. E. Collier, J. M. Fedeyko, H. Jobson, R. R. Rajaram, *Catal. Today* **2014**, *231*, 56–63.
[12] J. H. Kwak, D. Tran, S. D. Burton, J. Szanyi, J. H. Lee, C. H. F. Peden, *J. Catal.* **2012**, *287*, 203–209.
[13] C. W. Andersen, M. Bremholm, P. N. R. Vennestrøm, A. B. Blichfeld, L. F. Lundegaard, B. B. Iversen, *IUCrJ* **2014**, *1*, 382–386.
[14] J. . Martens, A. Cauvel, F. Jayat, S. Vergne, E. Jobson, *Appl. Catal. B Environ.* **2001**, *29*, 299–306.
[15] M. Moliner, J. E. Gabay, C. E. Kliewer, R. T. Carr, J. Guzman, G. L. Casty, P. Serna, A. Corma, *J. Am. Chem. Soc.* **2016**, *138*, 15743–15750.
[16] D. W. Fickel, E. D'Addio, J. A. Lauterbach, R. F. Lobo, *Appl. Catal. B Environ.* **2011**, *102*, 441–448.
[17] U. Deka, A. Juhin, E. A. Eilertsen, H. Emerich, M. A. Green, S. T. Korhonen, B. M. Weckhuysen, A. M. Beale, *J. Phys. Chem. C* **2012**, *116*, 4809–4818.
[18] S. I. Zones, *Zeolite SSZ-13 and Its Method of Preparation*, **1985**, US4544538.
[19] S. I. Zones, *J. Chem. Soc. Faraday Trans.* **1991**, *87*, 3709.
[20] M. Itakura, I. Goto, A. Takahashi, T. Fujitani, Y. Ide, M. Sadakane, T. Sano, *Microporous Mesoporous Mater.* **2011**, *144*, 91–96.
[21] H. Robson, K. P. Lillerud, Eds. , in *Verif. Synth. Zeolitic Mater.*, Elsevier Science, Amsterdam, **2001**, pp. 123–125.
[22] S. I. Zones, R. A. Van Nordstrand, *Zeolites* **1988**, *8*, 166–174.
[23] Y. Ji, M. A. Deimund, Y. Bhawe, M. E. Davis, *ACS Catal.* **2015**, *5*, 4456–4465.
[24] L. Van Tendeloo, E. Gobechiya, E. Breynaert, J. A. Martens, C. E. A. Kirschhock, *Chem. Commun.* **2013**, *49*, 11737–11739.
[25] M. Itakura, I. Goto, A. Takahashi, T. Fujitani, Y. Ide, M. Sadakane, T. Sano, *Microporous Mesoporous Mater.* **2011**, *144*, 91–96.
[26] T. Takata, N. Tsunoji, Y. Takamitsu, M. Sadakane, T. Sano, *Microporous Mesoporous Mater.* **2016**, *225*, 524–533.
[27] N. Martín, M. Moliner, A. Corma, *Chem. Commun.* **2015**, *51*, 9965–9968.
[28] M. Itakura, T. Inoue, A. Takahashi, T. Fujitani, Y. Oumi, T. Sano, *Chem. Lett.* **2008**, *37*, 908–909.
[29] I. Goto, M. Itakura, S. Shibata, K. Honda, Y. Ide, M. Sadakane, T. Sano, *Microporous Mesoporous Mater.* **2012**, *158*, 117–122.
[30] M. Dusselier, M. E. Davis, *Chem. Rev.* **2018**, *118*, 5265–5329.
[31] S. Goel, S. I. Zones, E. Iglesia, *J. Am. Chem. Soc.* **2014**, *136*, 15280–15290.
[32] A. Corma, C. Li, M. Moliner, *Angew. Chemie* **2018**, DOI 10.1002/ange.201711422.
[33] A. Gallas-Hulin, J. Mielby, S. Kegnæs, *ChemistrySelect* **2016**, *1*, DOI 10.1002/slct.201600831.
[34] S. Altwasser, R. Gläser, A. S. Lo, P. Liu, K. Chao, J. Weitkamp, *Microporous Mesoporous Mater.* **2006**, *89*, 109–122.
[35] K. G. Strohmaier, in *Zeolites Catal. Prop. Appl.*, The Royal Society Of Chemistry, **2017**, pp. 73–102.
[36] M. Choi, Z. Wu, E. Iglesia, *J. Am. Chem. Soc.* **2010**, *132*, 9129–9137.
[37] N. Wang, Q. Sun, R. Bai, X. Li, G. Guo, J. Yu, *J. Am. Chem. Soc.* **2016**, *138*, 7484–7487.
[38] Z. Wu, S. Goel, M. Choi, E. Iglesia, *J. Catal.* **2014**, *311*, 458–468.
[39] S. Goel, Z. Wu, S. I. Zones, E. Iglesia, *J. Am. Chem. Soc.* **2012**, *134*, 17688–17695.
[40] J. O. Abildstrøm, M. Kegnæs, G. Hytoft, J. Mielby, S. Kegnæs, *Microporous Mesoporous Mater.* **2016**, *225*, 232–237.
[41] B. N. Bhadra, P. W. Seo, N. A. Khan, J. W. Jun, T.-W. Kim, C.-U. Kim, S. H. Jhung, *Catal. Today* **2017**, *298*, 53–60.
[42] K. Honda, A. Yashiki, M. Itakura, Y. Ide, M. Sadakane, T. Sano, *Microporous Mesoporous Mater.* **2011**, *142*, 161–167.
[43] X. Xiong, D. Yuan, Q. Wu, F. Chen, X. Meng, R. Lv, D. Dai, S. Maurer, R. McGuire, M. Feyen, et al., *J. Mater. Chem. A* **2017**, *5*, 9076–9080.
[44] S. Goel, S. I. Zones, E. Iglesia, *Chem. Mater.* **2015**, *27*, 2056–2066.
[45] T. Maruo, N. Yamanaka, N. Tsunoji, M. Sadakane, T. Sano, *Chem. Lett.* **2014**, *43*, 302–304.
[46] W. H. Baur, *Am. Mineral.* **1964**, *49*, 697–704.
[47] M. Calligaris, G. Nardin, L. Randaccio, *Zeolites* **1983**, *3*, 205–208.
[48] J. O. Abildstrøm, Z. N. Ali, U. V. Mentzel, J. Mielby, S. Kegnæs, M. Kegnæs, *New J. Chem.* **2016**, *40*, 4223–4227.
[49] W. P. Davey, *Phys. Rev.* **1925**, *25*, 753–761.
[50] F. N. Ridha, Y. Yang, P. A. Webley, *Microporous Mesoporous Mater.* **2009**, *117*, 497–507.
[51] J. Shang, G. Li, R. Singh, P. Xiao, J. Z. Liu, P. A. Webley, *J. Phys. Chem. C* **2010**, *114*, 22025–22031.
[52] J. Zečević, A. M. J. van der Eerden, H. Friedrich, P. E. de Jongh, K. P. de Jong, *ACS Nano* **2013**, *7*, 3698–3705.
[53] T. Visser, T. A. Nijhuis, A. M. J. van der Eerden, K. Jenken, Y. Ji, W. Bras, S. Nikitenko, Y. Ikeda, M. Lepage, B. M. Weckhuysen, *J. Phys. Chem. B* **2005**, *109*, 3822–3831.
[54] G. Bergeret, P. Gallezot, in *Handb. Heterog. Catal.* (Eds.: G. Ertl, H. Knözinger, F. Schüth, J. Weitkamp), **2008**, pp. 738–765.
[55] M. Bourgogne, J.-L. Guth, R. Wey, *Process for the Preparation of Synthetic Zeolites, and Zeolites Obtained by Said Process*, **1985**, US Patent 4 503 024.

10.1002/cctc.201800914

WILEY-VCH

FULL PAPER

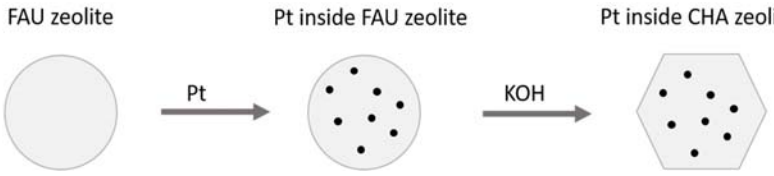

*Kristoffer Hauberg Rasmussen, Jerrik Mielby, and Søren Kegnæs**

Page No. – Page No.

Simple encapsulation strategy for Pt in chabazite

Platinum nanoparticles of 1-2 nm in size were trapped in a commercially available FAU zeolite by simple impregnation. The platinum particles were captured in a small pore CHA zeolite by interzeolite transformation of the Pt containing FAU zeolite using only potassium hydroxide solution at mild conditions. The catalyst prepared from this route showed high catalytic activity in oxidation of CO to CO_2.